Effect of the Hydrophobic Component on the Properties of Sulfonated Poly(arylene ether sulfone)s

Byungchan Bae, Kenji Miyatake,* and Masahiro Watanabe*

Fuel Cell Nanomaterials Center, University of Yamanashi, 4 Takeda, Kofu 400-8510, Japan

Received November 26, 2008; Revised Manuscript Received January 24, 2009

ABSTRACT: Four kinds of sulfonated poly(arylene ether sulfone)s containing hydrophobic component of different size was synthesized by the copolymerization of disodium 3,3′-disulfo-4,4′-difluorophenyl sulfone and 4,4′-difluorophenyl sulfone with 2,2-bis(2-hydroxy-5-biphenylyl)propane (SPE1), 4,4′-dihydroxytetraphenylmethane (SPE2), 9,9-bis(4-hydroxyphenyl)fluorene (SPE3), or 2,7-dihydroxynaphthalene (SPE4) under nucleophilic aromatic substitution conditions. The copolymer composition was set at 45−70 mol % of 3,3′-disulfo-4,4′-difluorophenyl sulfone in order to achieve similar ion exchange capacity (ca. 2.0 mequiv/g) for all the sulfonated copolymers SPE1−4. The copolymers were of high molecular weight (M_n = 150−220 kDa, M_w = 310−695 kDa) to give tough and flexible membranes by solution casting. STEM observation revealed that small hydrophobic components (SPE3 and SPE4) induced larger water cluster than bulky hydrophobic ones (SPE1 and SPE2). The small hydrophobic components induced high proton conductivities and proton diffusion coefficients as well as low water swelling. SPE4 membrane showed the highest proton conductivity at 50−80 °C and 10−90% RH among the four SPEs membranes. The smaller hydrophobic component was also effective in terms of gas permeation and mechanical properties for fuel cell applications.

Introduction

Polymer electrolyte membrane fuel cells (PEMFCs) have been studied as a clean source of energy due to high energy efficiency and no carbon dioxide emission. Their application ranges from mobile electronic devices to electric vehicles and stationary power sources.[1] Polymer electrolyte membranes are one of the key components in PEMFCs and perfluorosulfonic acid (PFSA) polymers have been the state-of-the-art materials. The PFSA, however, suffers from several problems such as high production cost and environmental inadaptability, which has prompted research on nonfluorinated ionomer membranes. Aromatic polymers bearing acid functions are a possible candidate to replace PFSA polymers. Such polymers include sulfonated poly(arylene ether sulfone)s,[2,3] poly(arylene ether ether ketone)s,[4−6] poly(arylene sulfide sulfone)s,[7] polyimides,[8] polyphosphazenes,[9] polybenzimidazoles,[10] and polyphenylenes.[11] While significant improvement has been achieved by appropriate molecular design, these ionomers membranes are not yet suitable for practical applications in terms of proton conductivity and long-term stability.

In order to develop high performance PEMs, more detailed understanding on the relationship between structures and properties should be obtained. Typical sulfonated aromatic polymers are composed of two components, hydrophilic and hydrophobic moieties. The former contains sulfonic acid groups and contributes to water affinity and proton conduction. In addition to the acid concentration or ion exchange capacity (IEC), its acidity is a crucial factor to determine the number of the effective protons taking part in proton conduction; i.e., a higher acidity of sulfonic acid groups leads to higher concentrations of mobile protons due to an increased number of dissociated protons. Moreover, the high acidity could enhance phase separation between hydrophilic and hydrophobic phases due to the increased polarity of hydrophilic components, and thus resulted in better connection of proton transporting pathway.[12] On the other hand, hydrophobic component plays a role in maintaining mechanical strength and dimensional stability of the membranes under fuel cell operating (wet and heated) conditions. The challenge is how to consolidate the opposite functions of each component by optimizing molecular structure. A number of approaches have been proposed for the purpose, which include introducing bulky and rigid hydrophobic moieties or polar substituents[13,14] and block or graft copolymers[15−18] and reinforcing with inorganic fillers.[19,20] These approaches have been well reviewed in the literature.[21,22]

Recently, we have reported that poly(arylene ether sulfone)s containing sulfofluorenyl groups are highly proton conductive and durable for 5000 h in operating fuel cells.[23] It is assumed that fluorenyl groups render good water holding capability and high proton conductivity under high humidity conditions. However, the conductivity at low humidity still needs to be improved. We herein report the effect of chemical structure of the hydrophobic component on the properties of the sulfonated poly(arylene ether sulfone) membranes. A series of sulfonated poly(arylene ether sulfone)s with different hydrophobic component, isopropylidene bis(biphenylene) (SPE1), diphenylmethylene biphenylene (SPE2), fluorenylidene biphenylene (SPE3), and 2,7-naphthylene (SPE4), were prepared, in which the approximate molecular size of the hydrophobic components was estimated via semiempirical molecular orbital calculation to be in the order SPE1 > SPE2 and SPE3 > SPE4 (Figure 1). Even

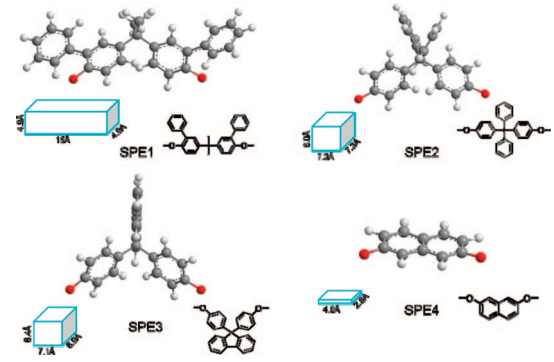

Figure 1. Optimized structure and approximate molecular size of the hydrophobic component.

* Corresponding author. Telephone: +81 55 220 8620. E-mail: m-watanabe@yamanashi.ac.jp.

10.1021/ma8026518 CCC: $40.75
Published on Web 02/20/2009

though ionomers from the dihydroxyl groups have been reported by different groups,[12,24,25] extensive studies about the effect of the hydrophobic components are needed in order to design optimized structure for PEMs. The morphology, water absorbability, proton conductivity, gas permeability and mechanical properties of the SPEs membranes were investigated.

Experimental Section

Materials. 4,4′-Difluorophenyl sulfone (FPS) was purchased from TCI, Inc. and crystallized from toluene before use. 2,2-Bis(2-hydroxy-5-biphenylyl)propane (BHBP), 4,4′-dihydroxytetraphenylmethane (DHTPM), 9,9-bis(4-hydroxyphenyl)fluorene (BHF), and 2,7-dihydroxynaphthalene (DHNT) were purchased from TCI., Inc. and crystallized from toluene/ethanol. Fuming sulfuric acid (30 wt % SO_3), potassium carbonate, and toluene were purchased from Kanto Chemical Co. and used as received. N,N-dimethyl acetamide (DMAc, organic synthesis grade, 99%) was purchased from TCI., Inc. and dried over 3 Å molecular sieves prior to use. Nafion NRE-212 membrane was purchased from du Pont and treated with 5 wt % H_2O_2 aqueous solution for 1 h and boiling 1 M H_2SO_4 aqueous solution for 1 h, and washed several times with deionized water.

Synthesis of Disodium 3,3′-disulfo-4,4′-difluorophenyl Sulfone (SFPS). Synthesis of SFPS was followed by the method of Robeson et al.[26] A 500 mL round-bottomed flask was charged with fuming sulfuric acid (200 mL) and FPS (100 g). The mixture was heated at 120 °C for 12 h with magnetic stirring. It was poured dropwise into a large excess of cold saturated NaCl aqueous solution. The precipitate was collected by filtration, dissolved in water and neutralized with NaOH aqueous solution. Addition of NaCl gave a precipitate of the crude product, which was purified by recrystallization three times from water/ethanol solution (2/8 by volume) and dried in vacuum oven at 120 °C. Pure SFPS was obtained in 60% yield. ^{1}H NMR (DMSO-d_6): δ (ppm) 8.16 (d, 2H), 7.97 (t, 2H), 7.43 (d, 2H).

Polymerization. A typical polymerization procedure is as follows. A 100 mL round-bottomed flask was charged with SFPS (6.0 mmol), FPS (2.57 mmol), BHBP (8.57 mmol), potassium carbonate (17.14 mmol), 20 mL of DMAc, and 10 mL of toluene. SFPS was predried overnight at 120 °C in vacuum oven in order to remove hydrated water. The reaction was carried out at 140 °C for 4 h with Dean−Stark trap. Then, the temperature was elevated to 165 °C and the reaction was continued for 24 h to obtain light yellow viscous solution. The mixture was diluted with 20 mL of additional DMAc and poured dropwise into a large excess of water. The crude product was washed with deionized water and methanol several times. It was dissolved in DMSO and filtrated with 0.45 μm membrane filter. Acetone was added to the filtrate to precipitate high molecular weight polymer. The polymer was collected with filtration and dried in vacuum oven to obtain SPE1. The other copolymers, SPE2, -3, and -4, were synthesized in a similar manner.

Membrane Preparation. SPEs (1 g) in DMAc (20 mL) solution were cast onto a flat glass plate. Drying the solution at 60 °C for overnight gave a 50 ± 5 μm thick, transparent, and tough film. The films were further dried in a vacuum oven at 80 °C for at least 6 h. The membranes were converted to the proton form by immersion in 1 M H_2SO_4 aqueous solution for 4 h, followed by washing with water several times and drying at 60 °C.

Measurements. ^{1}H NMR spectra were obtained on a Bruker AVANCE 400S using deuterated dimethyl sulfoxide (DMSO-d_6) as a solvent and tetramethylsilane (TMS) as an internal reference. Ion exchange capacity (IEC) of SPEs membranes was calculated from the peak area in the ^{1}H NMR spectra. Titration was also used for the determination of IEC. A piece of SPE membrane was equilibrated in large excess of 0.05 M NaCl aqueous solution for overnight. The released HCl by the ion exchange was titrated with standard 0.01N NaOH aqueous solution. Molecular weight was measured with gel permeation chromatography (GPC) equipped with two Shodex KF-805 columns and a Jasco 805 UV detector with DMF containing 0.01 M LiBr as eluent. Molecular weight was calibrated with standard polystyrene samples. Density of dry SPEs and Nafion membranes was measured by a pycnometer (Ultrapycnometer1000, Quantachrome Inc.) using helium as test gas at room temperature. Density at 50, 80, and 110 °C was calibrated by use of the volume expansion coefficient of perfluoroalkyl polymer (PFA: 1.3×10^{-4} K^{-1}) and poly(ether sulfone) (PSF: 3.1×10^{-4} K^{-1}), since the coefficients of sulfonated polymers were not available. The density of water at 110 °C was regarded as the same as that at 100 °C.

For scanning transmission electron microscopy (STEM) observations, sulfonic acid groups of the membranes were stained with silver ion by immersing overnight in 0.5 M $AgNO_3$ aqueous solution, rinsing with deionized water, and drying in vacuum oven for 12 h. The stained membranes were embedded in epoxy resin, sectioned to 90 nm thickness with Leica microtome Ultracut UCT, and placed on copper grids. Images were taken on a Hitachi HD-2300C STEM with an accelerating voltage of 200 kV.

Water uptake and proton conductivity were measured with a solid electrolyte analyzer system (MSBAD-V-FC, Japan Bel Co.) equipped with a temperature and humidity controllable chamber. Humidification and dehumidification cycles from 10% to 90% RH were repeated 3 times, and data from the first cycle were excluded. At least 2 samples of each SPE membrane were tested and 4 different data points (2 cycles per each test) were averaged to obtain water uptake and proton conductivity. Deviation of each sample was found to be within ± 5%. Vacuum drying for 3 h at 80 °C gave the weight of dry membranes and exposure to a given humidity for at least 3 h gave the weight of hydrated membranes. Weight of the membranes was measured by magnetic suspension balance at given humidity and then, water uptake ((weight of hydrated membrane − weight of dry membrane)/weight of dry membrane × 100) was calculated. Proton conductivity was measured using 4-probe conductivity cell attached with impedance spectroscopy (Solartron 1255B and 1287, Solartron Inc.). Ion conducting resistances (R) were determined from the impedance plot obtained in the frequency range from 1 to 10^5 Hz. The proton conductivity (σ) was calculated from the equation, $\sigma = l/A \cdot R$, where A and l are the conducting area and the membrane thickness, respectively. Hysteresis of water uptake and proton conductivity at given humidity was calculated by subtracting the sorption value from the desorption value. Increase of humidity gave the sorption value and decrease of humidity gave the desorption value.

From the conductivity and density data, the proton diffusion coefficient (D_σ) was calculated using the Nernst−Einstein equation (eq 1)

$$D_\sigma = \frac{RT}{F^2}\frac{\sigma}{c(H^+)} \tag{1}$$

where R is gas constant, T is the absolute temperature (K), F is Faraday constant, and $c(H^+)$ is the concentration of the proton charge carrier (mol/L).

Hydrogen and oxygen permeability was measured with a gas permeation measurement apparatus (20XFYC, GTR-Tech Inc.) and concentration of the permeated gases was quantified with a gas chromatography (GC, G2700T, Yanaco) with thermal conductivity detector. Argon and helium were used as a carrier for the measurement of hydrogen and oxygen, respectively. Membranes were placed in the center of the permeation cell and the test gas was introduced onto one side of the membrane at a flow rate of 20 mL/min. Carrier gas was introduced onto the other side of the membrane at the same flow rate and was analyzed by the GC. The same humidity conditions were applied to both test and carrier gases to ensure homogeneous wetting of the membrane samples. The membrane was equilibrated at least 3 h before each measurement. The five data were averaged in each experiment. The gas permeation rate, r (cm^3 (STD) cm^{-2} s^{-1}) and the gas permeability coefficient, Q (barrer = 1×10^{-10} cm^3 (STD) cm cm^{-2} cm^{-1} mmHg^{-1}), was calculated by eqs 2 and 3, respectively

$$r = \frac{273}{T} \times \frac{1}{A} \times B\frac{1}{t} \tag{2}$$

$$Q = \frac{273}{T} \times \frac{1}{A} \times B \times \frac{1}{t} \times l \times \frac{1}{76 - P_{water}} \quad (3)$$

where T (K) is the absolute temperature, A (cm^2) is the permeation area, B (cm^3) is the volume of the test gas permeated through the membrane, t (s) is the sampling time, l (cm) is the thickness of the membrane, and P_{water} (cmHg) is the water vapor pressure.

Tensile strength was measured by universal test machine (AGS-J 500N, Shimadzu) attached with temperature and humidity controllable chamber (Bethel-3A, Toshin Kogyo). Stress vs strain curves were obtained for samples cut into a dumbbell shape (DIN-53504-S3, 35 mm × 6 mm (total) and 12 mm × 2 mm (test area)). Measurement was conducted at 93% RH and 85 °C at a stretching speed of 10 mm/min.

Results and Discussion

Synthesis and Characterization of SPE1, -2, -3, and -4. The four biphenols, BHBP, DHTPM, BHF, and DHNT, were chosen as hydrophobic comonomers. These biphenols could be polymerized with SFPS and FPS in a manners similar to that reported in the literature[2,27] to give the corresponding sulfonated copolymers, SPE1−4 (Scheme 1, in which X represents mole percentage of the hydrophilic component containing sulfonic acid groups). The feed monomer ratio was determined as $X = 70$ (SPE1), 68 (SPE2), 70 (SPE3), and 45 (SPE4) in order that the copolymers have similar IEC values (ca. 2.0 meq/g). The four SPEs were obtained as fibers with good solubility in polar organic solvents such as DMSO, DMF, and DMAc. The chemical structure of the SPEs was investigated with ^{1}H NMR spectra (Figure 2). The ^{1}H NMR spectra of the SPE1, -2, -3, and -4 were well-assigned to the proposed chemical structure. The copolymer composition was calculated from the integration ratio of the peaks to obtain the IEC values. As summarized in Table 1, the experimental IEC values obtained from titration and ^{1}H NMR spectra were in near accordance with the ones expected from the feed monomer ratio. The results indicate that the copolymerization reaction was complete and the sulfonic acid groups in the membranes act as ion exchange sites. The SPEs were of high molecular weight with $M_n > 150$ kDa and $M_w > 310$ kDa. Casting the DMAc solution gave tough, ductile and flexible membranes. Among the three SPEs containing similar X values (68−70), SPE1 membrane showed the lowest density (1.31 g/cc) due to the bulkiest hydrophobic component. We discuss the effect of hydrophobic component on the membrane morphology in the following section.

Morphology. Morphologies of the SPEs membranes were investigated by STEM observation (Figure 3). At least 2 samples by a different batch and 3 different spots were investigated in the observation. All of the SPEs membranes showed a reproducible tendency, and selected images are shown in this figure. In these images, black spot represents hydrophilic domain containing sulfonic acid groups, being exchanged with silver ions. As a comparison, STEM image of the Nafion NRE-212 membrane is also presented where well-developed phase separation with hydrophilic clusters of ca. 4−6 nm size were observed. For SPEs membranes, smaller hydrophilic clusters were confirmed throughout the observed images. Despite their similar IEC values, the four SPEs membranes differ in the morphologies. The hydrophilic clusters became bigger with decreasing size of the hydrophobic component (from SPE1 to SPE4). Thus, SPE4 membrane showed the largest hydrophilic clusters (∼6 nm), implying the most pronounced separation between hydrophobic and hydrophilic phases. It is considered that small and planar naphthylene groups are likely to aggregate and accordingly facilitate aggregation of the hydrophilic component. In contrast, smaller and well-dispersed hydrophobic domains were observed for the SPEs with larger hydrophobic components (especially SPE1 and SPE2).

Scheme 1. Synthesis of SPE1, SPE2, SPE3, and SPE4[a]

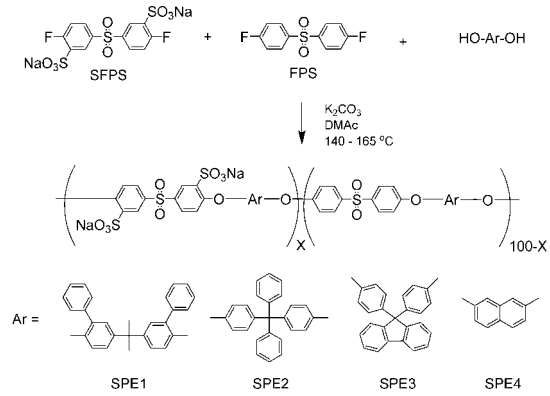

[a] X represents mol % of the sulfonated component.

Water Uptake and Proton Conductivity. Water uptake of the SPEs and Nafion NRE-212 membranes were measured at 50, 80, and 110 °C, and were plotted as a function of relative humidity (RH) in Figure 4a. The measurements were carried out by repeating sorption (humidifying) and desorption (dehumidifying) processes (the data in Figure 4 were obtained during the desorption process, and hysteresis between the desorption and sorption will be discussed in the next section). The water uptake of the SPEs was higher than that of Nafion at the temperatures and humidities examined due to the formers' higher IEC value. Among the SPEs, SPE1 showed the highest water uptake. This is possibly due to weaker intermolecular interaction of the SPE1 with the bulkiest hydrophobic component compared to those of the other SPEs. The STEM image in Figure 3 revealed less developed hydrophilic clusters in SPE1 membrane, which would be related to less aggregation of the hydrophobic component. The water uptake data were converted to the number of absorbed water molecules per sulfonic acid groups (λ), and were plotted as a function of temperature at 20, 40, and 60% RH in Figure 4b. Nafion membrane showed higher λ values than that of the SPEs over the whole range of temperature and humidities, which implied higher water affinity. Both SPEs and Nafion membranes showed decreasing λ as increasing temperature at constant water activity. The results indicate that the water holding capability of these polymer electrolytes decreases at high temperature. However, the tendency was different above 80 °C between Nafion and SPEs membranes. Nafion showed a slight increase in λ at 110 °C, whereas SPEs showed an almost linear decrease in λ from 50 to 110 °C. This could be explained by an much lower glass transition temperature of Nafion (ca. 110 °C in dry and lower in wet) than that of the wholly aromatic polymer electrolytes (the latter do not show glass transition behavior below their decomposition temperatures).

Figure 5a shows the proton conductivity of the SPEs and Nafion NRE-212 membranes. Due to random structure of the SPE membranes, high IEC is required in order to obtain comparable conductivity to that of Nafion. Recently block copolymers have been suggested to overcome this shortcoming.[28−30] The proton conductivity of the SPEs membranes was more dependent on the humidity than that of Nafion. Although the proton conductivity of SPEs was comparable to Nafion at high RH (>80%), it decreased by several orders of magnitude with decreasing RH. It is due to the less developed phase separation in SPEs membranes than that of the perfluorinated ionomer membranes and often observed for aromatic polymer electrolytes.[31] Despite its highest water uptake, SPE1 membrane showed the lowest proton conductivity. This result is not

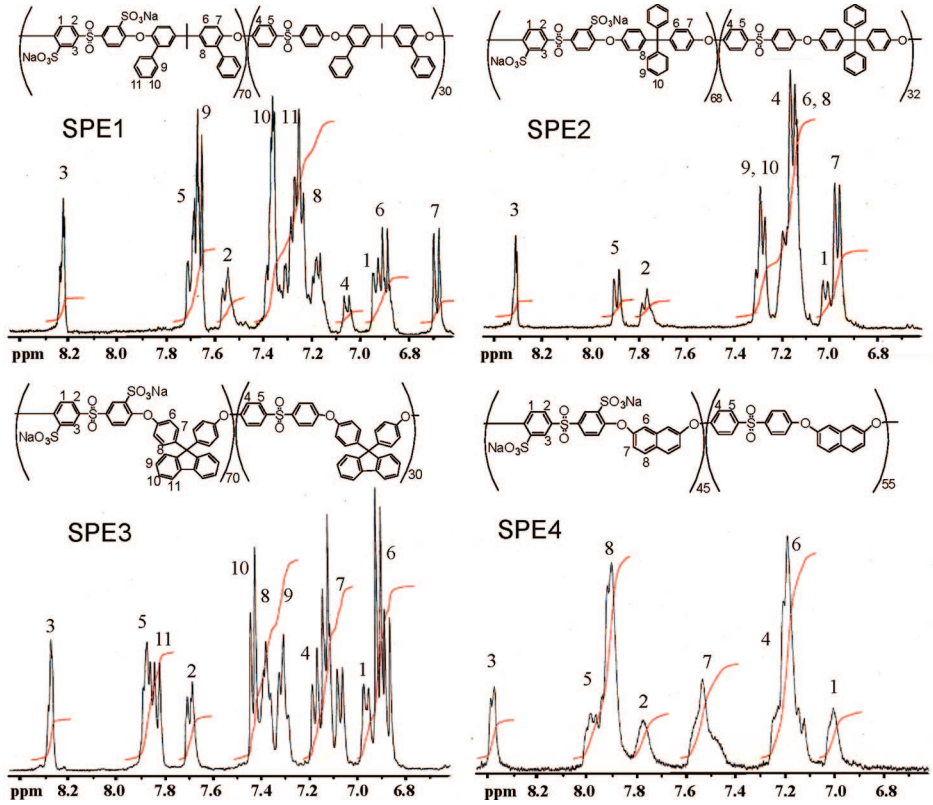

Figure 2. ^{1}H NMR spectra of SPE1, SPE2, SPE3, and SPE4 in DMSO-d_6.

Table 1. Mole Percentage, IEC, Molecular Weight, and Density of the SPEs Membranes

		IEC (mequiv/g)					
			experimental				
SPE	X^a	expected	titration	NMR	M_n (kDa)	M_w (kDa)	density (g/cm^3)^b
SPE1	70	1.98	2.00	1.91	192	411	1.31
SPE2	68	2.01	1.98	1.93	215	360	1.37
SPE3	70	2.07	1.93	1.97	150	310	1.39
SPE4	45	2.01	1.90	1.94	220	695	1.38

^{a} Mole percentage of the SFPS containing component. ^{b} At 25 °C.

contradictory with the STEM images. The bulky hydrophobic component induced less phase separation and accordingly lower proton conductivity. In other words, the absorbed water did not effectively contribute to the proton conduction. The SPE4 membrane, on the other hand, showed relatively higher proton conductivity in spite of its lower water uptake, which is well accordance with results of Xing et al.[32]

The proton conductivity was plotted as a function of temperature at 20, 40, and 60% RH in Figure 5b. The Nafion membrane showed nearly Arrhenius type temperature dependence of the proton conductivity, indicating that the similar proton conduction mechanism at 50−110 °C. The SPE membranes showed maxima of the proton conductivity at ca. 80 °C, 40 and 60% RH. The conductivity decreased as increasing temperature at 20% RH. The decrease in the proton conductivity of SPEs membranes at high temperature and/or low humidity would result from the lowered λ values ($\leq$3) in Figure 4b, at which most of the water molecules are strongly bound to the sulfonic acid groups. Another plausible reason is that SPEs membranes have less-connected proton transporting pathway under such conditions. The results suggest that better connection of hydrophilic domains is crucial for the sulfonated poly(arylene ether sulfone) membranes in order to achieve further improvement of the proton conductivity at low humidity and high temperature.

From the data in Figures 4 and 5, proton diffusion coefficients could be calculated by use of the Nernst−Einstein equation regarding water volume and concentration of proton charge carrier in polymer electrolyte membranes. Figure 6 shows proton diffusion coefficients (D_σ) as a function of water volume fraction (Φ) at 50, 80, and 110 °C. Similar to the proton conductivity, D_σ of the Nafion was higher than that of the SPEs and the difference between the Nafion and SPEs became larger at lower Φ. Among the SPEs, SPE3 and SPE4 showed relatively higher D_σ values than those of SPE1 and SPE2. The results are reasonable taking their morphology (Figure 3) into account. It is generally recognized that proton transfer is based on the Grotthuss (proton hopping through hydrogen bonds) and vehicle mechanisms (migration of hydronium ions) at low temperature. At high temperature, the vehicle mechanism dominates over the Grotthuss mechanism.[33] Even if this is the case or not, it is evident that well-developed and connected hydrophilic clusters are crucial for proton conduction especially at low humidity (low water content).

Hysteresis Behavior of Water Uptake. During the measurement of water uptake and proton conductivity, hysteresis behavior was observed between sorption and desorption processes. At each temperature and humidity, the membranes were equilibrated for at least 3 h before the measurement was carried out. The difference (λ_{DS} - λ_S) in λ between sorption (λ_S) and desorption (λ_{DS}) processes is defined as the hysteresis value and plotted as a function of RH in Figure 7. The SPEs and Nafion

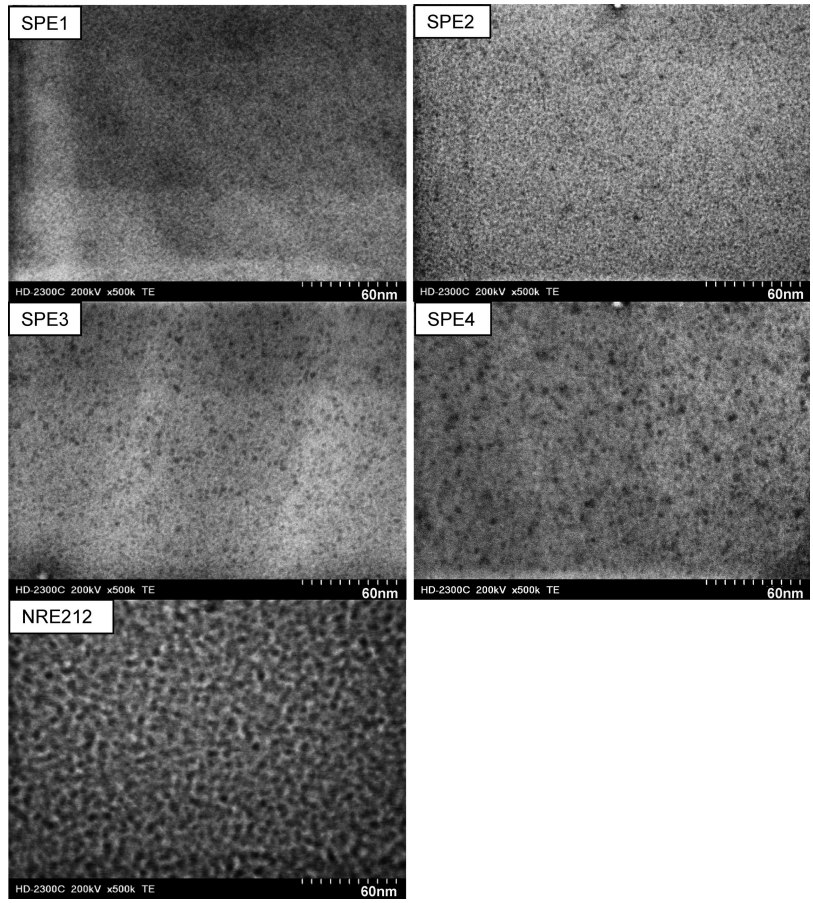

Figure 3. Cross-sectional STEM images of silver-ion stained SPEs and Nafion NRE-212membranes.

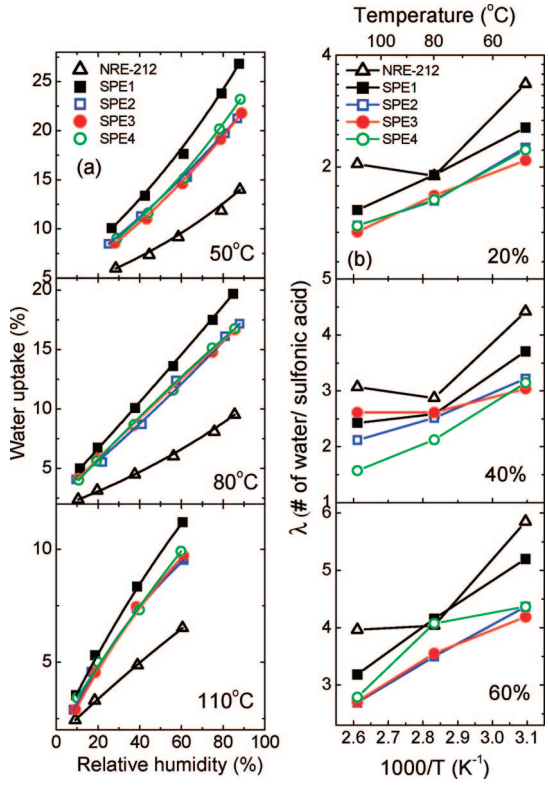

Figure 4. (a) Water uptake at 50, 80, and 110 °C, and (b) temperature dependence of λ at 20, 40, 60% RH of SPEs and Nafion NRE-212 membranes. Data were taken during the desorption process.

membranes showed positive hysteresis values. The hysteresis values of SPEs were higher than those of Nafion. The hysteresis values became even higher at increasing RH (except at 80 °C and 80% RH). The results indicate that it took much longer time for SPEs than Nafion until the membranes were equilibrated with the environment since the former are composed of rigid aromatic structures. The wide and well-connected hydrophilic channels in Nafion would also be responsible. Among the SPEs membranes, SPE4 showed relatively lower hysteresis compared to the other SPEs. This is not contradictory to the STEM image in Figure 3, in which rather larger and developed hydrophilic clusters were observed. With increasing temperature, the hysteresis became lower for all SPEs due to the increased molecular motion. Similar behavior was observed under high humidity conditions (80 °C and 80% RH), where softening of the membranes was probably occurring.

Gas Permeability. Hydrogen and oxygen permeability of the SPEs and Nafion membranes was measured under dry conditions and plotted as a function of temperature in Figure 8. All SPEs showed lower hydrogen and oxygen permeability and lower activation energy than that of Nafion membrane. The apparent activation energy of the gas permeability of Nafion was $E_a(H_2) = 38$ and $E_a(O_2) = 52$ kJ/mol and that of the SPEs were $E_a(H_2) = 12-17$ and $E_a(O_2) = 13-22$ kJ/mol. The similar activation energy among the SPEs implied the same gas transport mechanism. It should be noted that the SPE4 membrane showed the lowest hydrogen and oxygen permeability. Both hydrophobic and hydrophilic domains are responsible for the gas permeation in ionomer membranes, while Piroux et al. have reported that the contribution of hydrophilic domains on the gas permeation is negligible compared to the hydrophobic under dry conditions.[34] This tendency was more pronounced for higher IEC

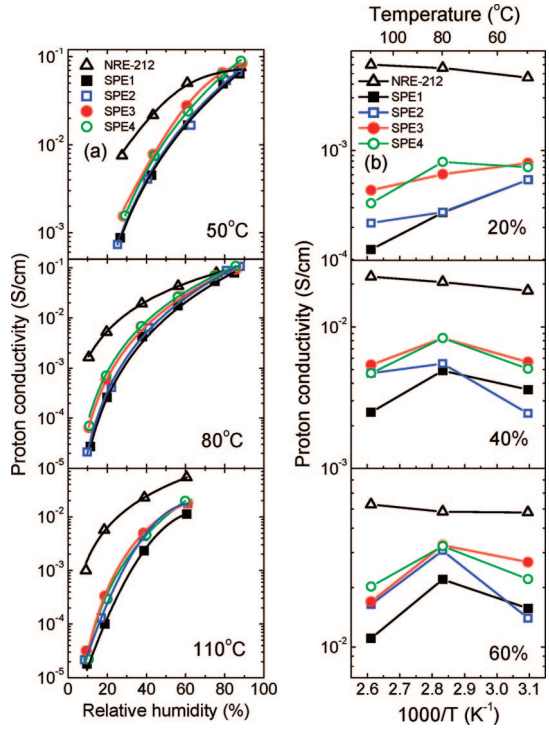

Figure 5. (a) Humidity dependence and (b) temperature dependence of the proton conductivity of SPEs and Nafion membranes. Data were taken during the desorption process.

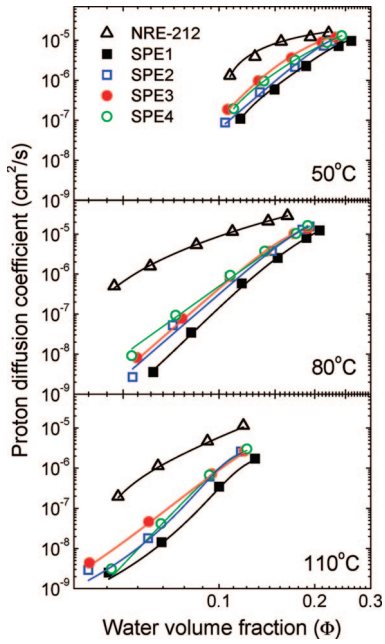

Figure 6. Proton diffusion coefficient of SPEs and Nafion NRE-212 membranes as a function of water volume fraction at 50, 80, and 110 °C.

membranes. The gas permeability of the SPEs under dry conditions would be mainly contributed from the free volume in hydrophobic domains. Thus, the lowest gas permeability of the SPE4 membrane is reasonable for its flat naphthylene structure as hydrophobic component. For the applications at high temperature PEMFCs with lower gas permeability and lower activation energy are favorable.

Figure 9 shows hydrogen and oxygen permeability under humidified conditions at 80 °C. At any humidity, the SPEs showed lower gas permeability than that of Nafion. However, the humidity dependence of the gas permeability was different between SPEs and Nafion membranes. Hydrogen and oxygen permeability of the SPEs decreased slightly at initial stages of humidification (30% RH) and then increased with further humidification. The behavior of hydrogen permeability is consistent with that of the sulfonated polyimide membranes of which the determining factor changed with the amount of absorbed water.[34] When membranes are contacted with water vapor, water molecules are absorbed by sulfonic acid groups, which results in decrease in the free volume and gas permeation of SPEs. The contribution of the hydrophilic component to gas permeation is not striking at low RH since the hydrophilic channel is still under development. With further humidification, the membranes absorb more water molecules and begin to develop hydrophilic clusters along with connectivity. Then, the contribution from the hydrophilic domains becomes larger to cause an increase in the total gas permeability of the membranes. At higher RH, hydrophilic domains dominate gas permeation. The behavior is not observed for the Nafion membrane due to its highly developed water channels even at low RH. Similar to the results under dry conditions, SPE4 showed the lowest gas permeability among the four SPEs membranes. A significant increase in gas permeation for the SPEs membranes from 30 to 90% RH reflect their larger water uptake values at humidity as shown in Figure 4a.

Mechanical Properties. Elongation of SPEs was tested at 93% RH and 85 °C by a universal test instrument. The hydrophobic component had a major impact on the mechanical properties of SPEs membranes as in stress versus strain curves (Figure 10). As shown in Figure 10, each membrane showed different Young's modulus and elongation at break. SPE1 membrane showed the highest elongation at break (230%) due to high water uptake. The Young's modulus of SPE1 estimated from the slope was 11 MPa. The SPEs membranes became stiffer with decreasing size of the hydrophobic component; initial Young's modulus of SPE2, -3, and -4 were 31, 133, and 146 MPa, respectively. The results support our claim that the smaller hydrophobic component caused more developed hydrophobic and hydrophibic phase separation. The developed

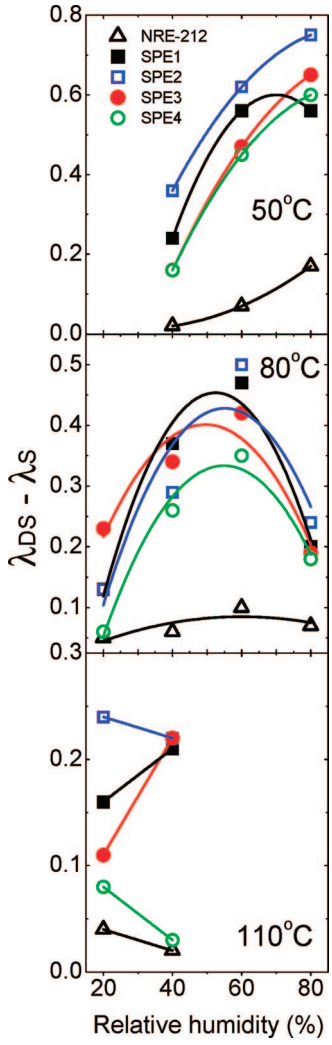

Figure 7. Humidity dependence of hysteresis ($\lambda_{DS} - \lambda_S$) of SPEs and Nafion NRE-212 membranes at 50, 80, and 110 °C.

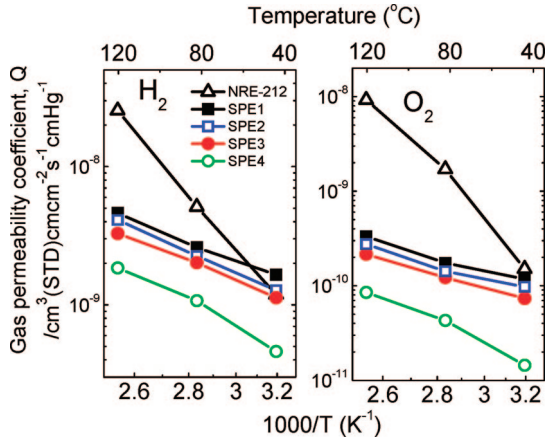

Figure 8. Temperature dependence of hydrogen and oxygen permeability of SPEs and Nafion NRE-212 membranes under dry conditions.

phase separation resulted in higher Young's modulus of the SPE3 and -4 membranes. SPE3 and SPE4 showed peaks after initial elongation and then showed steady elongation, whereas SPE1 and SPE2 did not show such peaks. Liu et al. also observed similar behavior in their SPE (BPSH) at high elongation rate.[35] They interpreted this behavior as onset of disentanglement of the bundles in hydrophobic component. Since

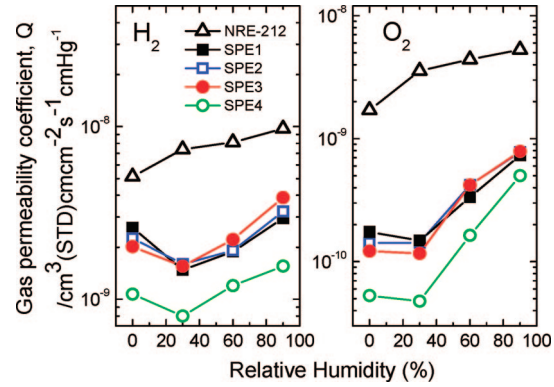

Figure 9. Humidity dependence of hydrogen and oxygen permeability of SPEs and Nafion NRE-212 membranes at 80 °C.

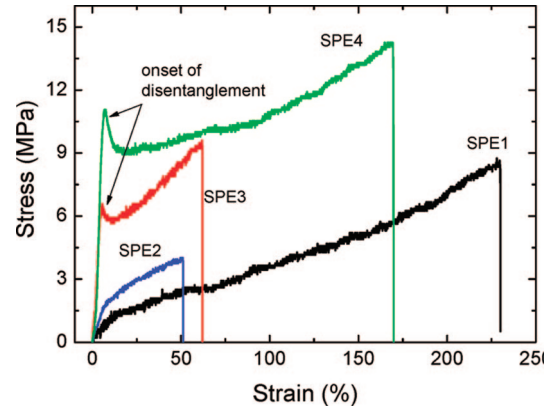

Figure 10. Strees vs strain curves of SPEs and Nafion NRE-212 membranes at 85 °C and 93% RH.

the elongation rate was fixed at 10 mm/min for all SPEs in our elongation test, this different behavior of SPE3 and SPE4 may be attributable to hydrophobic component. It would be reasonable to assume that the SPE3 and 4 contain larger amounts of hydrophobic bundles to show the onset peak of the disentanglement.

Conclusions

The effect of the hydrophobic component on the properties of sulfonated poly(arylene ether sulfone)s was investigated. The smaller hydrophobic components, such as planar naphthylene groups induced larger and more developed hydrophilic clusters, whereas larger ones such as isopropylidene bis(biphenylene) caused smaller and dispersed hydrophilic domains. The developed hydrophilic clusters were effective for high proton conductivity and low water uptake. The small hydrophobic component was also favorable for low gas permeability and high mechanical strength. For the PEMFC applications, we concluded that small hydrophobic component was preferable. However, the proton diffusion coefficient of the SPEs membranes was still much lower than that of Nafion and needs to be improved for higher proton conductivity at low water content.

Acknowledgment. This work was partly supported by the New Energy and Industrial Technology Development Organization (NEDO) through the HiPer-FC Project, and the Ministry of Education, Culture, Sports, Science and Technology (MEXT) Japan through a Grant-in-Aid for Scientific Research (20350086).

References and Notes

(1) Kordesch, K.; Simader, G., *Fuel cells and their applications*. VCH: Weinheim, Germany, 1996.

(2) Wang, F.; Hickner, M.; Kim, Y. S.; Zawodzinski, T. A.; McGrath, J. E. *J. Membr. Sci.* **2002**, *197*, 231–242.
(3) Chikashige, Y.; Chikyu, Y.; Miyatake, K.; Watanabe, M. *Macromolecules* **2005**, *38*, 7121–7126.
(4) Xing, P.; Robertson, G. P.; Guiver, M. D.; Mikhailenko, S. D.; Wang, K.; Kaliaguine, S. *J. Membr. Sci.* **2004**, *229*, 95–106.
(5) Gil, M.; Ji, X.; Li, X.; Na, H.; Eric Hampsey, J.; Lu, Y. *J. Membr. Sci.* **2004**, *234*, 75–81.
(6) Shang, X.; Tian, S.; Kong, L.; Meng, Y. *J. Membr. Sci.* **2005**, *266*, 94–101.
(7) Schuster, M.; Kreuer, K.-D.; Andersen, H. T.; Maier, J. *Macromolecules* **2007**, *40*, 598–607.
(8) Miyatake, K.; Zhou, H.; Matsuo, T.; Uchida, H.; Watanabe, M. *Macromolecules* **2004**, *37*, 4961–4966.
(9) Guo, Q.; N; Pintauro, P.; Tang, H.; O'Connor, S. *J. Membr. Sci.* **1999**, *154*, 175–181.
(10) Wainright, J. S.; Wang, J.-T.; Weng, D.; Savinell, R. F.; Litt, M. *J. Electrochem. Soc.* **1995**, *142*, L121.
(11) Fujimoto, C. H.; Hickner, M. A.; Cornelius, C. J.; Loy, D. A. *Macromolecules* **2005**, *38*, 5010–5016.
(12) Bae, B.; Miyatake, K.; Watanabe, M. *J. Membr. Sci.* **2008**, *310*, 110–118.
(13) Miyatake, K.; Zhou, H.; Uchida, H.; Watanabe, M. *Chem. Commun.* **2003**, 368–369.
(14) Kim, Y. S.; Kim, D. S.; Liu, B.; Guiver, M. D.; Pivovar, B. S. *J. Electrochem. Soc.* **2008**, *155*, B21−B26.
(15) Matsumura, S.; Hlil, A. R.; Lepiller, C.; Gaudet, J.; Guay, D. ; Shi, Z.; Holdcroft, S.; Hay, A. S. *Macromolecules* **2008**, *41*, 281–284.
(16) Lee, H.-S.; Roy, A.; Lane, O.; Dunn, S.; McGrath, J. E. *Polymer* **2008**, *49*, 715–723.
(17) Schöberger, F.; Kerres, J. *J. Polym. Sci., Part A: Polym. Chem.* **2007**, *45*, 5237–5255.
(18) Kim, D. S.; Robertson, G. P.; Guiver, M. D. *Macromolecules* **2008**, *41*, 2126–2134.
(19) Kim, Y. S.; Wang, F.; Hickner, M.; Zawodzinski, T. A.; McGrath, J. E. *J. Membr. Sci.* **2003**, *212*, 263–282.
(20) Miyatake, K.; Tombe, T.; Chikashige, Y.; Uchida, H.; Watanabe, M. *Angew. Chem., Int. Ed.* **2007**, *46*, 6646–6649.
(21) Hickner, M. A.; Ghassemi, H.; Kim, Y. S.; Einsla, B. R.; McGrath, J. E. *Chem. Rev.* **2004**, *104*, 4587–4612.
(22) Hamrock, S. J.; Yandrasits, M. A. *Polym. Rev.* **2006**, *46*, 219–244.
(23) Asano, N.; Aoki, M.; Suzuki, S.; Miyatake, K.; Uchida, H.; Watanabe, M. *J. Am. Chem. Soc.* **2006**, *128*, 1762–1769.
(24) Brunelle, D. J.; Zhou, H.; Liu, H.; Hung, J.; Harmon, M. E.; Moore, D. R. Sulfonated polyaryletherketone-block-polyethersulfone copolymers. WO/2008/005647, **2008**.
(25) Gao, Y.; Robertson, G. P.; Guiver, M. D.; Mikhailenko, S. D.; Li, X.; Kaliaguine, S. *Polymer* **2006**, *47*, 808–816.
(26) Robeson, L. M.; Matzner, M. *Flame retardant polyarylate compositions.* US Patent 4,380,598, **1983**.
(27) Bai, Z.; Dang, T. D. *Macromol. Rapid Commun.* **2006**, *27*, 1271–1277.
(28) Meier-Haack, J.; Taeger, A.; Vogel, C.; Schlenstedt, K.; Lenk, W.; Lehmann, D. *Sep. Purif. Technol.* **2005**, *41*, 207–220.
(29) Ghassemi, H.; McGrath, J. E.; Zawodzinski, J. T. A. *Polymer* **2006**, *47*, 4132–4139.
(30) Sumiko Matsumura, A. R. H.; Allan, S. Hay. *J. Polym. Sci. Part A: Polym. Chem.* **2008**, *46*, 6365–6375.
(31) Kreuer, K. D. *J. Membr. Sci.* **2001**, *185*, 29–39.
(32) Xing, P.; Robertson, G. P.; Guiver, M. D.; Mikhailenko, S. D.; Kaliaguine, S. *J. Polym. Sci. Part A: Polym. Chem.* **2004**, *42*, 2866–2876.
(33) Ren, X.; Gottesfeld, S. *J. Electrochem. Soc.* **2001**, *148*, A87−A93.
(34) Piroux, F.; Espuche, E.; Mercier, R. *J. Membr. Sci.* **2004**, *232*, 115–122.
(35) Liu, D.; Kyriakides, S.; Case, S. W.; Lesko, J. J.; Li, Y.; McGrath, J. E. *J. Polym. Sci. Part B: Polym. Phys.* **2006**, *44*, 1453–1465.

MA8026518